Pure Appl. Geophys.

https://doi.org/10.1007/s00024-023-03317-8

Pure and Applied Geophysics

Contribution of Solar Irradiance Variations to Surface Air Temperature Trends at Different Latitudes Estimated from Long-term Data

Igor I. Mokhov[1,2] and Dmitry A. Smirnov[1,3]

Abstract—Contributions of the insolation variations together with different natural and anthropogenic factors to the trends of the surface air temperatures at different latitudes of the Northern and Southern Hemispheres on various temporal horizons are estimated from climate data since the nineteenth century with the use of empirical autoregressive models. As the natural climate variability modes, we take into account Atlantic Multidecadal Oscillation, El-Nino/Southern Oscillation, Interdecadal Pacific Oscillation, Pacific Decadal Oscillation, and Antarctic Oscillation. According to the obtained results, the contributions of the insolation variations to the trends of the surface air temperature are statistically insignificant on the time intervals under study, i.e. from a decade and longer. Taking into account the insolation variations in the autoregressive models weakly alters the estimates of the contributions of the greenhouse gases and natural variability modes to the temperature trends: the changes are not more than several per cent. Numerically, the estimated contributions of the insolation variations can considerably exceed the respective contributions of the natural variability modes both on short (less than two decades) and long (longer than a century) time intervals.

Keywords: Surface temperature trends, Contributions of insolation variations, Greenhouse gases, Natural variability modes, Time series analysis, Autoregressive models, Granger causality and medium-term causality.

1. Introduction

Climate change is one of the key global problems. An overall increase of the global surface air temperature (GST) is revealed from the observation data since the nineteenth century, each of the last four decades has been warmer than any previous decade (Masson-Delmotte et al., 2021). More than a half of this increase during last decades is attributed to the anthropogenic rise of the atmospheric content of the greenhouse gases (GHGs) (Bindoff et al., 2013). In the time range from several years to several decades, natural variability can also essentially enhance or weaken the global warming. To achieve more adequate predictions of global and regional climate changes, one needs various quantitative estimates of the contributions of natural and anthropogenic factors to such changes. The significant impact of the GHGs has been inferred from empirical data in many studies in comparison with various natural factors such as solar and volcanic activity and "internal" quasi-cyclic processes (Masson-Delmotte et al., 2021; Stocker et al., 2013; Santer et al., 2001; Allen et al., 2006; Kaufmann et al., 2006, 2011; Lockwood, 2008; Foster & Rahmstorf, 2011; Kopp & Lean, 2011; Loehle & Scafetta, 2011; Gruza & Rankova, 2012; Zhou & Tung, 2013; Stern & Kaufmann, 2014; Stolpe et al., 2017; Mokhov & Smirnov, 2018a, 2018b; Kajtar et al., 2019; McBride et al., 2021). In particular, Tung and Camp (2008) estimated the amplitude of the global warming related to the 11-year solar cycle to be about 0.2 K with greater warming over the polar regions than over the tropics, and (Lean & Rind, 2008) obtained that the El Niño phenomena induce the GST changes up to 0.2 °C on the time scales of several years, considerable volcanic eruptions–up to 0.3 °C, and solar activity variations–about 0.1 °C, see also (Lean & Rind, 2009; Mokhov & Smirnov, 2008). Many works confirm significance of the GHGs impact on GST and compare it with the impact of other factors, see e.g. (Tol & de Vos, 1993; Kaufmann & Stern, 1997; Verdes, 2007; Lean &

[1] A.M. Obukhov Institute of Atmospheric Physics of the Russian Academy of Sciences, 3 Pyzhevsky Per., 119017 Moscow, Russia. E-mail: smirnovda@yandex.ru

[2] Department of Physics, Lomonosov Moscow State University, Leninskie Gory, 119991 Moscow, Russia.

[3] Saratov Branch, Kotelnikov Institute of Radioengineering and Electronics of the Russian Academy of Sciences, 38 Zelyonaya Street, 410019 Saratov, Russia.

Published online: 08 July 2023

Rind, 2008; Mokhov & Smirnov, 2009; Smirnov & Mokhov, 2009; Attanasio &Triacca, 2011; Kodra et al., 2011; Mokhov et al., 2012; Imbers et al., 2013; Triacca et al., 2013; Mokhov & Smirnov, 2016a, 2016b; Stips et al., 2016; Mokhov & Smirnov, 2022).

The possibility of compensation for the global warming due to a potentially significant weakening of the insolation in the future was studied, e.g., in (Mokhov et al., 2006, 2008; Feulner & Rahmstorf, 2010; Song et al., 2010; Jones et al., 2012; Anet et al., 2013; Meehl et al., 2013; Maycock et al., 2015; Arsenovic et al., 2018). Thus, estimates of the climate change under various scenarios of changes in solar and volcanic activity and anthropogenic forcings for the twenty-first century were made in (Mokhov et al., 2006, 2008) with the use of ensemble simulations with a global climate model taking into account the carbon cycle. In particular, the estimates were obtained for scenarios with extreme weakening of insolation, comparable to the Maunder and Dalton minima. The results of ensemble simulations indicated a weak contribution of the solar irradiance variations to the change in the global surface air temperature in the twenty-first century in comparison with the possible anthropogenic forcings. According to the results of model simulations with the GHG increase in the atmosphere in (Song et al., 2010), the effect of multidecadal solar variations on climate depends on the GHG content. The authors noted a possibility of an increase of the regional climate response to the solar irradiance decrease due to a change in the climate variability modes, though the warming caused by the GHG increase cannot be compensated even by a possible large solar minimum.

To develop the above mentioned studies, it is necessary to assess the contributions of different factors to the temperature trends for different areas of the Earth on different time scales. Thus, in (Mokhov & Smirnov, 2022) we have used a simple method based on multivariate autoregressive (AR) models to estimate the contributions of GHGs and several natural modes of climate variability (Atlantic Multidecadal Oscillation–AMO, El Niño/Southern Oscillation–ENSO, Interdecadal Pacific Oscillation–IPO, Pacific Decadal Oscillation–PDO, and Antartic Oscillation–AAO also called Southern Annular Mode–SAM) to the temperature trends at different latitudinal belts of the Northern Hemisphere (NH) and the Southern Hemisphere (SH) on different time intervals, with a special attention to the intervals of about half a century and shorter which is principally important to resolve many questions in climate science.

As the next step, we investigate to what extent inclusion of the solar activity variations into the AR models can change the previously obtained estimates of the contribution of various factors to the temperature trends on different time intervals in different regions. The method used here for estimating the contributions to trends is based on the concept of stochastic dynamical models and medium-term causal effects (Mokhov & Smirnov, 2022) similar to the idea of long-term causality which has been suggested in (Mokhov & Smirnov, 2009; Smirnov & Mokhov, 2009) and found its further development within the framework of dynamical causal effects (Smirnov, 2014, 2022). Relation of this method to the well-known "fingerprints" approach (Allen & Stott, 2003; Allen & Tett, 1999; Hasselmann, 1993, 1997; Hegerl & Zwiers, 2011; Hegerl et al., 1996; Huntingford et al., 2006; Imbers et al., 2014; Jia & DelSole, 2012; Ribes & Terray, 2013; Ribes et al., 2009) is discussed in (Mokhov & Smirnov, 2022).

2. *Data*

For the present analysis, we have used the mean annual data for the surface air temperature anomalies T relative to the reference period 1971–2000 at different latitudes as shown in Fig. 1a and b. Different colors represent tropical (0–30°N), middle (30–60°N), and Arctic (60–90°N) latitudes of the NH and the corresponding (0–30°S, 30–60°S, and 60–90°S) latitudes of the SH. These are the land–ocean temperatures since 1880 till now from the ERSST (Extended Reconstruction of Sea Surface Temperatures) version 4 (Huang et al., 2014; Liu et al., 2014; Huang et al., 2015). Due to the deficiencies of the data for the Antarctic latitudes, the respective estimates possess rather a qualitative character.

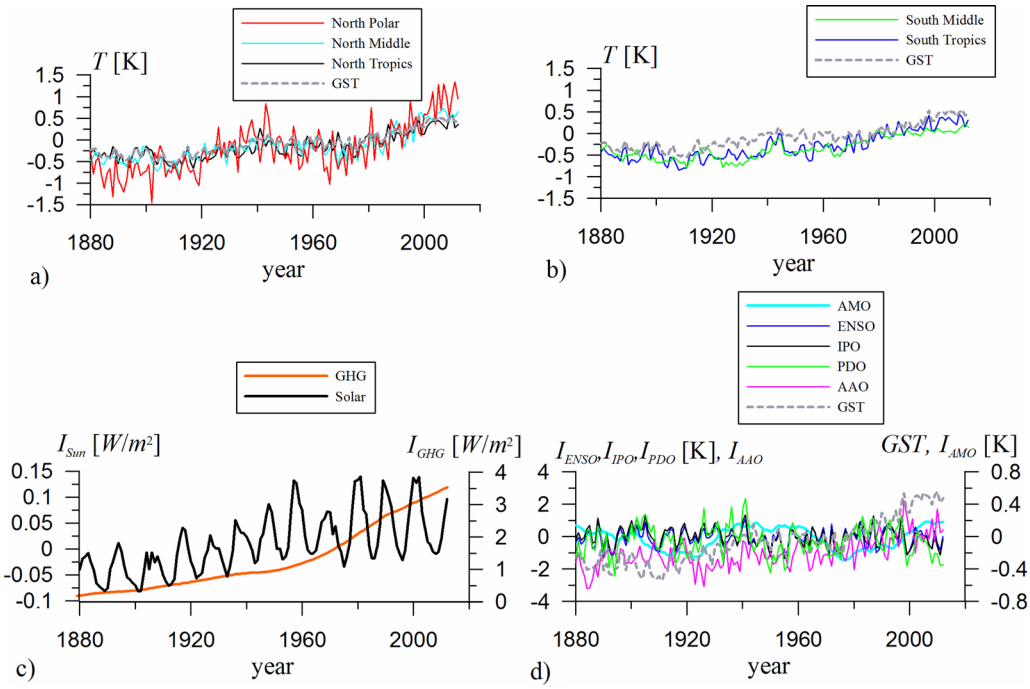

Figure 1
Time series under analysis which represent interannual variations of the following indices: **a**, **b** the surface air temperature T at various latitudes of the NH and the SH (different colors are explained in the legend) and for the entire Earth (GST, grey dashes, shown for the data visualization purposes only); **c** the solar activity (black) and GHGs radiative forcing (brown); **d** indices of the filtered AMO (cyan), ENSO (blue), IPO (black), PDO (green), and AAO (magenta)

Interannual variations of the solar and GHGs radiative forcings under the analysis are shown in (Fig. 1c). These are the data since the nineteenth century till 2012 used in GISS CMIP5 simulations (Miller et al., 2014; GISS, 2018). The data used here for solar radiative forcing variations are discussed in detail in Sect. 3.6 of (Miller et al., 2014).

Selection of the indices of AMO, ENSO, IPO, PDO, and AAO (Fig. 1d; PSL, 2022) for the analysis is determined by the attempt to include a long-term internal variability associated with Pacific Ocean (ENSO, IPO, PDO) and Atlantic Ocean (AMO) or with processes in the antarctic and subantarctic latitudes (AAO) into empirical AR models for the temperature variations.

The AMO is an ongoing series of long-duration changes in the sea surface temperature of the North Atlantic Ocean, with cool and warm phases that may last for several decades at a time. The detrended AMO index since 1856 till now from the HadISST1 data set (Enfield et al., 2001; Rayner et al., 2003) is used here. This index is currently calculated over the latitudes north of equator. However, for comparisons to the previous results (Mokhov & Smirnov, 2018a, 2018b, 2022), we have used the previous version of the index computed for the band 20°N–70°N (Fig. 1d, cyan). In any case, this index possesses the characteristic periodicity of about 6 decades.

We have used a slow component of the index which is represented by the annual-mean values of the index smoothed with a weighted moving average filter with a 10-year triangular window. The choice of the filter is discussed in (Smirnov & Mokhov, 2015) and used also in (Mokhov & Smirnov, 2018a, 2018b, 2022).

The ENSO is characterized by strong interannual fluctuations in the sea surface temperature of the equatorial Pacific Ocean with the associated atmospheric pressure anomalies over the Pacific. The ENSO index which shows sea surface temperature anomalies in the region Nino-3,4 (5°S–5°N,

170–120°W) is used here (Fig. 1d, blue). These data since 1870 till now are based on the HadISST1 data set.

The PDO is a key mode of interdecadal climate variability in the NH over the Pacific related with the El Niño phenomena. The PDO index based on the ERSST version 5 (NCEI, 2022) is used here. The data cover the interval since 1854 till now (Fig. 1d, green).

The IPO characterizes interdecadal climate variability over a wide Pacific area in the Northern and Southern Hemispheres. Its index called TPI (tripole index) and used here is defined as the difference between the sea surface temperature of the central equatorial Pacific (10°S–10°N, 170°E–90°W) and the mean sea surface temperature of the north-western (25°N–45°N, 140°E–145°W) and south-western (50°S–15°S, 150°E–160°W) Pacific (Henley et al., 2015). The data last since 1870 till now (Fig. 1d, black).

The AAO is a mode of the atmospheric pressure field in the SH which is characterized by the difference of the sea level pressure between 40 and 65°S (Gong & Wang, 1999). The data for that index used here cover the period since 1871 till 2012 (Fig. 1d, magenta).

We have fitted all empirical models below to the period since 1880 till 2012 where each of the 13 mentioned variables is available.

3. Method

Various contributions to the temperature trends for each latitudinal zone are estimated on time intervals of the lengths ranging from 5 to 130 years with the aid of empirical multivariate AR models analogously to (Mokhov & Smirnov, 2018a, 2018b, 2022). The approach fits to the framework of dynamical causal effects (Mokhov & Smirnov, 2022; Smirnov, 2014; Smirnov & Mokhov, 2009) based on the comparison of dynamics of a model under alternative conditions. Under that approach, one considers a coupled stochastic (Markovian) dynamical system consisting of two subsystems X and Y. To characterize an effect of coupling in the direction $Y \to X$, one performs some variation in the initial state or parameters of the subsystem Y and examines the response of the subsystem X at some future time instant or on some future time interval in an appropriate sense which provides the corresponding dynamical causal effect. Here, the effect of interest is defined as a response of X (a change of the linear trend of an observable x on some future time interval) when the dynamics of Y is changed from an observed time series of y to an alternative regime where y is equal to a constant value starting from a certain time instant. This is a kind of the parameter variation as explained in (Smirnov, 2022). So, from the dynamical causal effects viewpoint, the contribution to the trend belongs to the family "parameter variation–medium-term effect" (Smirnov, 2022).

In this work, we construct a model for each temperature anomaly T taking into account the influences of the GHGs, solar activity, and a natural variability mode I_M in the form

$$T_n = a_0 + a_1 T_{n-1} + a_2 I_{GHG,n-1} + a_3 I_{M,n-1} + a_4 I_{Sun,n-1} + \xi_n \quad (1)$$

Here, n is discrete time (years), ξ_n is white noise (it corresponds to a variability with time scales of about a year and less), I_{GHG} is the GHGs radiative forcing, I_M is the index of a climate mode, and I_{Sun} is the solar radiative forcing. The index I_M is either I_{AMO}, or I_{ENSO}, or I_{IPO}, or I_{PDO}, or I_{AAO}. Only one of the natural variability indices I_M is included into the model (1) to keep it as small as possible and so retain reasonable statistical properties of the estimates. The evolution equations for I_{GHG}, I_M, and I_{Sun} are not constructed, since these factors are considered here as external drivers. The AR Eq. (1) is fitted to the entire observation interval via the ordinary least-squares technique, i.e. via minimization of the sum $S(\mathbf{a}) = \sum \xi_n^2$ of squared errors $\xi_n = T_n - a_0 - a_1 T_{n-1} - d_2^n I_{GHG,n-1} - a_3 I_{M,n-1} - a_4 I_{Sun,n-1}$ over the parameter vector $\mathbf{a}$. The least-squares estimates $\hat{a}_0, \hat{a}_1, \hat{a}_2, \hat{a}_3, \hat{a}_4$ are obtained along with the estimates of their standard deviations. The latters are available from the same regression estimation under the assumption of a stationary white finite-variance noise and equal to the mean squared residual error multiplied by the inverse of $A^T A$ where A is the matrix whose columns are time series of the five regressors. Significance level at

which the null hypothesis of a zero coefficient is rejected is estimated as the inverse of the standard Gaussian cumulative distribution function evaluated at the estimated value of a coefficient divided by its estimated standard error. The residual errors corresponding to the least-squares estimate $\hat{\mathbf{a}} = (\hat{a}_0, \hat{a}_1, \hat{a}_2, \hat{a}_3, \hat{a}_4)$ are denoted $\hat{\xi}_n$. Agreement of the residuals with the white noise assumption is illustrated in Fig. 2 which presents the residuals versus discrete time n (upper panels) and their empirical autocorrelation functions with 95% confidence bands (lower panels). For the model (1) with AMO illustrated in Fig. 2a only the correlation at the lag of 4 years is significant at the pointwise level of $p < 0.05$ (more precisely, at $p = 0.15$). Taking into account Bonferroni multiple test correction, the ACF is significantly nonzero only at $p = 0.06$. Moreover, this ACF is about 0.2, i.e. still quite small. So, the procedure used here for the estimation of the model coefficient errors is justified. An attempt to include a more complex correlation structure of the residuals into the estimation procedure is not expected to change anything and to improve reliability of the results. Still, it can be performed at the future steps to check whether such details can lead to any changes of the estimation results. The residuals properties are overall similar for the models (1) with the other climatic modes, in particular, the results for ENSO are shown in Fig. 2b.

To determine the contributions of the anthropogenic and natural factors to the linear temperature trends for each of the six latitudinal zones over a time interval $[L_{start}, L_{end}]$ with the length $L = L_{end} - L_{start}$, we analyzed time realizations of the AR model (1) with the estimated parameters $\hat{\mathbf{a}}$ in hypothetical regimes for the natural variability modes or the GHGs atmospheric content: instead of the observed time series for a given factor (say, for the solar radiative forcing $I_{Sun,n}$, $n = 1880, \ldots, 2012$) we "fed" the model (1) with an artificially generated time series $\tilde{I}_{Sun,n}$ at its input. The initial value of T and the entire time series of the other two factors (i.e. of $I_{GHG,n}$ and $I_{M,n}$,$n = 1880, \ldots, 2012$, if the contribution of $I_{Sun,n}$ is estimated) at the model input were taken to equal the actually observed values. The time series of the "external noise" ξ_n at the model input was taken to

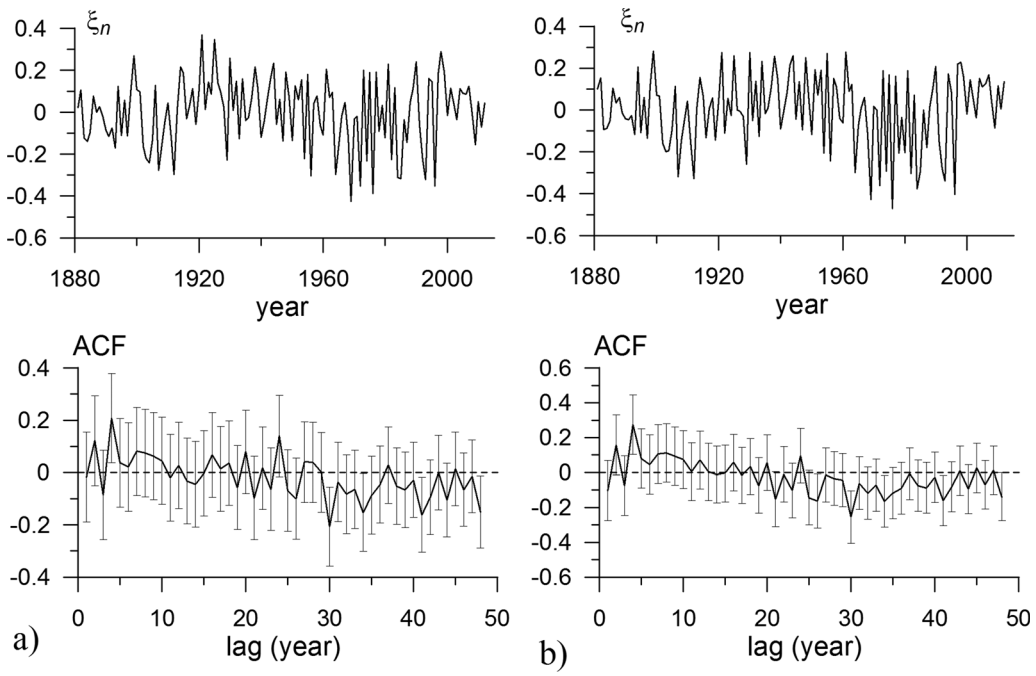

Figure 2
Model residuals (upper panels) and their empirical autocorrelation functions (lower panels) with 95% confidence bands estimated as ACF $\pm 2/\sqrt{N - lag}$ where $N = 132$ is the number of residuals. Both resilduals and ACFs are shown for the empirical models (1) where T is the temperature of the northern middle latitudes and the climatic mode is AMO (**a**) or ENSO (**b**)

be the time series of $\hat{\xi}_n$. The contribution of each factor to the trend was estimated as the difference between the trends of the actually observed values T_n and the model values $\tilde{T}_n$ obtained under the alternative condition (i.e. under the input signal $\tilde{I}_{Sun,n}$ in our example). It means that the model (1) is assumed to be applicable under that alternative condition. In this work, we take the hypothetical behavior to be a constant value $\tilde{I}_{Sun,n} = const$ or $\tilde{I}_{GHG,n} = const$ or $\tilde{I}_{M,n} = const$ (i.e. "absence of any dynamics") after some starting time instant, and take an unchanged behavior $\tilde{I}_{Sun,n} = I_{Sun,n}$ or $I_{GHG,n} = \tilde{I}_{GHG,n}$ or $\tilde{I}_{M,n} = I_{M,n}$ before that time instant. For any mode I_M, that constant level is close to the empirical mean of I_M over the entire interval 1880–2012 and the starting time instant is the first instant n when the value $I_{M,n}$ gets close to that constant. For I_{GHG} or I_{Sun} which exhibit long-term trends over the entire period under study, the constant level is the value of I_{GHG} or I_{Sun} in the very beginning of the time series and so the starting time instant of the changed behavior for any of these two factors is 1880.

The difference of the two trends above is equal to the linear trend of the temperature difference $\delta T_n = T_n - \tilde{T}_n$ and the latter is estimated below. This trend on each time interval $[L_{start}, L_{end}]$ (with L ranging from 5 to 130 years) is represented by a coefficient $\alpha_{\delta T}$ of the standard linear regression $\delta T_n = \alpha_{\delta T} n + \zeta_n$ obtained via the ordinary least-squares technique. In this way, we have estimated the contributions to the temperature trends from the five factors denoting such contributions as C_{GHG} (from GHGs), C_{Sun} (from solar radiative forcing), C_{AMO} (from AMO), C_{ENSO} (from ENSO), C_{IPO} (from IPO), and C_{AAO} (from AAO). We have estimated also the actual trend of T, i.e. the coefficient α_T in the regression equation $T_n = \alpha_T n + \zeta_n$. To assess the relative role of each factor, we have used the corresponding ratios, i.e. C_{GHG}/α_T, C_{Sun}/α_T, C_{AMO}/α_T, C_{Sun}/C_{GHG}, and C_{Sun}/C_{AMO} for the model (1) with GHGs, solar activity, and AMO. Everything is analogous for the models with ENSO, IPO, PDO, and AAO instead of AMO.

The selection of the simplest form of the possible AR models (linear, unit-lag, with a single mode I_M) and the noise realization $\hat{\xi}_n$ to generate the hypothetical alternative behavior are justified in (Mokhov & Smirnov, 2022) as a reasonable starting step to assess the contributions to the trends from empirical data without any presumed theoretical hypotheses about the climate processes under study. Further studies with more complicated nonlinear empirical models, e.g. such as those in (Mukhin et al., 2021; Seleznev et al., 2019) are surely possible. Concerning the model consistency check, all models (1) here agree well with the observed dynamics which is justified analogously to (Mokhov & Smirnov, 2022).The relative standard deviation of a trend contribution estimate appears equal to the relative standard deviation of the respective AR coupling coefficient estimate. So, the uncertainties in the trend contribution estimates can be easily obtained from the model fitting results (see Table 1). As a further check for significance of the solar activity variations contribution, we have compared each AR model (1) and its trend contribution estimates to the respective estimates for the model without solar activity

$$T_n = a_0 + a_1 T_{n-1} + a_2 I_{GHG,n-1} + a_3 I_{M,n-1} + \xi_n \quad (2)$$

The AR models (2) were used for the estimation in (Mokhov & Smirnov, 2018a, 2018b, 2022).

For an additional illustration of the coupling analysis performed in this work, we have estimated the widely known Granger causality (Granger, 1963, 1969) in terms of the mean-squared prediction improvements (PIs), its other examples with climate data are given e.g. in (Attanasio & Triacca, 2011; Mokhov & Smirnov, 2008, 2009, 2016a, 2016b, 2017; Mokhov et al., 2011). To estimate the coupling $x \to T$ from a process x to a process T given several other processes $y_1, \ldots, y_K$, one minimizes the mean-squared errors of the equation for T in the $(K+2)$-variate AR model

$$\sigma_{in}^2 = \frac{1}{N-P} \sum_{n=N-P}^{N} \left(T_n - a_0 - \sum_{i=1}^{P} a_i T_{n-i} - \sum_{k=1}^{K} \sum_{i=1}^{P} c_{k,i} y_{n-i} - \sum_{i=1}^{P} b_i x_{n-i} \right)^2 \quad (3)$$

and the similar equation in the respective $(K+1)$-variate AR model with x excluded

Table 1

Estimates (rounded-off) of the coefficients a_2 and a_3 of the AR models (1) and (2) with 95% confidence intervals, Δa is the double standard error

Coefficients of AR models: for the GHGs (a_2) and for a natural variability mode (a_3)

Lat	AMO		ENSO		IPO		PDO		AAO	
	$a_2 \pm \Delta a_2$	$a_3 \pm \Delta a_3$	$a_2 \pm \Delta a_2$	$a_3 \pm \Delta a_3$	$a_2 \pm \Delta a_2$	$a_3 \pm \Delta a_3$	$a_2 \pm \Delta a_2$	$a_3 \pm \Delta a_3$	$a_2 \pm \Delta a_2$	$a_3 \pm \Delta a_3$
1	**0.34** ± 0.11 (**0.35** ± 0.10)	**0.70** ± 0.50 (**0.70** ± 0.50)	**0.30** ± 0.11 (**0.30** ± 0.10)	*0.09* ± 0.12 (*0.09* ± 0.12)	**0.30** ± 0.11 (**0.31** ± 0.10)	*0.08* ± 0.11 (*0.07* ± 0.11)	**0.31** ± 0.11 (**0.32** ± 0.10)	0.03 ± 0.07 (0.03 ± 0.07)	**0.31** ± 0.12 (**0.32** ± 0.11)	–0.015 ± 0.09 (–0.015 ± 0.09)
2	**0.21** ± 0.06 (**0.21** ± 0.06)	**0.44** ± 0.25 (**0.44** ± 0.25)	**0.16** ± 0.06 (**0.16** ± 0.05)	0.03 ± 0.06 (0.03 ± 0.06)	**0.16** ± 0.06 (**0.16** ± 0.05)	0.02 ± 0.05 (0.02 ± 0.05)	**0.16** ± 0.06 (**0.16** ± 0.06)	0.01 ± 0.03 (0.01 ± 0.03)	**0.15** ± 0.06 (**0.15** ± 0.06)	0.01 ± 0.04 (0.01 ± 0.04)
3	**0.15** ± 0.05 (**0.15** ± 0.05)	**0.23** ± 0.20 (**0.23** ± 0.20)	**0.14** ± 0.05 (**0.14** ± 0.05)	*0.04* ± 0.05 (*0.04* ± 0.05)	**0.13** ± 0.05 (**0.14** ± 0.05)	0.02 ± 0.05 (0.02 ± 0.05)	**0.13** ± 0.05 (**0.13** ± 0.05)	–0.00 ± 0.03 (–0.00 ± 0.03)	**0.14** ± 0.05 (**0.15** ± 0.05)	***–0.03*** ± 0.03 (***–0.03*** ± 0.03)
4	**0.16** ± 0.05 (**0.17** ± 0.05)	0.07 ± 0.18 (0.07 ± 0.18)	**0.17** ± 0.06 (**0.18** ± 0.06)	*0.04* ± 0.05 (*0.04* ± 0.05)	**0.16** ± 0.06) (**0.17** ± 0.06)	0.02 ± 0.04 (0.02 ± 0.05)	**0.15** ± 0.05 (**0.16** ± 0.05)	–0.00 ± 0.03 (–0.00 ± 0.03)	**0.17** ± 0.06 (**0.17** ± 0.05)	–0.02 ± 0.03 (–0.02 ± 0.03)
5	**0.06** ± 0.03 (**0.06** ± 0.03)	0.00 ± 0.10 (0.00 ± 0.10)	**0.06** ± 0.03 (**0.06** ± 0.03)	–0.00 ± 0.03 (–0.00 ± 0.03)	**0.06** ± 0.03 (**0.06** ± 0.03)	0.00 ± 0.02 (0.00 ± 0.02)	**0.06** ± 0.03 (**0.06** ± 0.03)	0.01 ± 0.02 (0.01 ± 0.02)	**0.05** ± 0.03 (**0.05** ± 0.03)	0.01 ± 0.02 (0.01 ± 0.02)
6	*0.07* ± 0.09 (**0.08** ± 0.07)	–0.05 ± 0.50 (–0.05 ± 0.50)	*0.07* ± 0.08 (**0.08** ± 0.07)	***–0.11*** ± 0.12 (***–0.11*** ± 0.12)	*0.07* ± 0.09 (**0.08** ± 0.07)	–0.05 ± 0.12 (–0.06 ± 0.12)	*0.07* ± 0.09 (**0.08** ± 0.07	–0.01 ± 0.07 (–0.01 ± 0.07)	*0.10* ± 0.11 (**0.11** ± 0.09)	–0.05 ± 0.10 (–0.05 ± 0.10)

The latitudinal zones are: 1–Arctic, 2–middle latitudes of NH, 3–tropics of NH, 4–tropics of SH, 5–middle latitudes of SH, 6–Antarctic. Fonts show significance levels at which the hypothesis of zero coefficient is rejected: bold font–at $p < 0.05$ (highly significant), bold italic–at $0.05 < p < 0.1$, italic–at $0.1 < p < 0.2$, normal–non-significant; a_2 has the units of $K/(Wm^{-2})$, a_3 is dimensionless except for AAO where it has the units of K. Upper numbers in each cell are for the AR models (1) with solar activity, lower numbers in parentheses correspond to the AR models (2) without solar activity

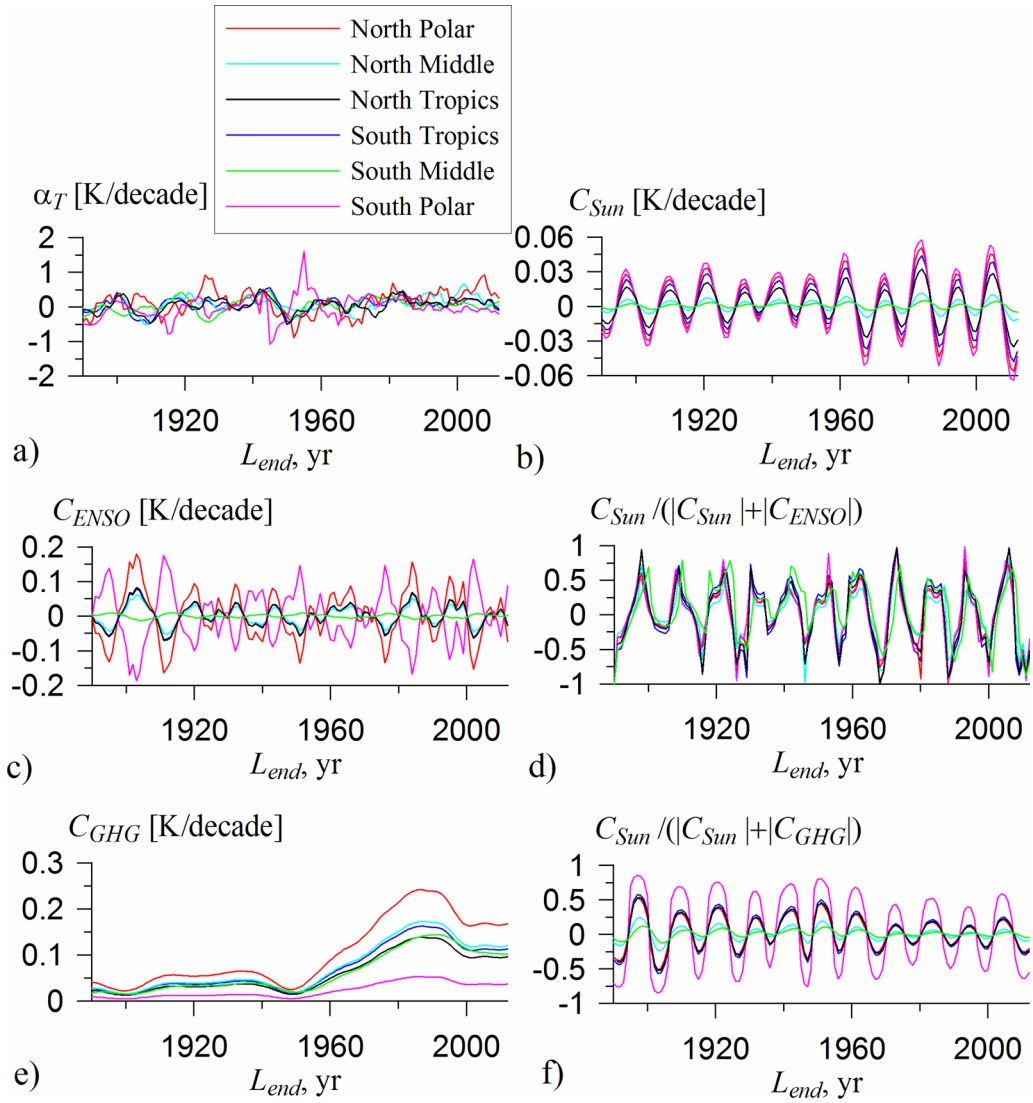

Figure 3
The temperature trends at different latitudes (see the legend) and the respective contributions of different factors within a 10-yr moving window versus the window end point: **a** the trends; **b** contributions of the solar activity according to the AR-models (1) accounting for ENSO; **c** contributions of ENSO; **d** contributions of the solar activity relative to the summed solar and ENSO contributions; **e** contributions of GHGs; **f** contributions of the solar activity relative to the summed solar and GHGs contributions

$$\sigma_{ex}^2 = \frac{1}{N-P}\sum_{n=N-P}^{N}\left(T_n - a_0 - \sum_{i=1}^{P} a_i T_{n-i} - \sum_{k=1}^{K}\sum_{i=1}^{P} c_{k,i} y_{n-i}\right)^2 \quad (4)$$

and computes e.g. the relative PI in the form $PI_{x\to T|y_1,\ldots,y_K} = \frac{\sigma_{ex}^2 - \sigma_{in}^2}{\sigma_{ex}^2}\cdot 100\ \%$. The AR order P is often selected with the use of the Schwarz information criterion (Schwarz, 1978). Nonzero PIs indicates that the coupling $x \to T$ is present. Statistical significance of this conclusion is often checked with the Fisher F-test. We have used $P = 1$ to present the Granger causality estimates for the same AR models as those used for the trend contributions estimation. Slightly greater values of P give similar results. The causality from GHGs to each of the six T's is presented below as $PI_{GHG\to T}$ for the bivariate AR models (3), i.e. with $K = 0$ and no other factors apart from GHGs, for brevity. The results are similar for greater

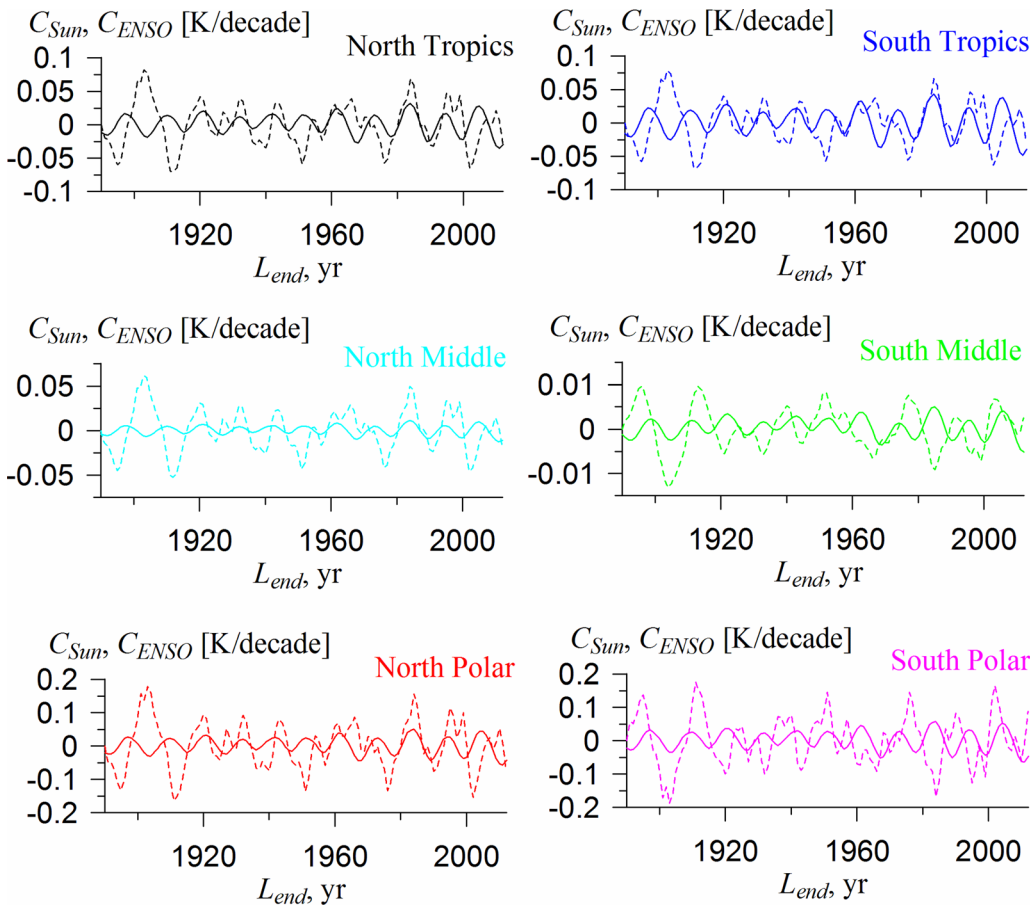

Figure 4
The contributions of the solar activity variations (solid lines) and ENSO (dashed lines) to the temperature trends within a 10-yrmoving window. Different panels correspond to different latitudes

values of K. The causality from the solar radiative forcing is presented for the trivariate AR models (3) with GHGs and solar activity, i.e. $PI_{Sun \to T|GHG}$ and $K = 1$. The causality from each natural mode M is presented for the full four-variate AR models (3) coinciding with the AR models (1), i.e. $PI_{M \to T|GHG,Sun}$ and $K = 2$.

4. Results

4.1. Relative Contributions of Solar Activity to Trends on Short Time Scales

After fitting the AR models (1) to the data under study, we have estimated contributions of GHGs, solar activity, and natural modes to the temperature trends. Since relative roles of the natural modes and solar activity are of the main interest in this work, let us start with an illustration of the typical results on short time scales of about 10 years. Figure 3 shows the temperature trends at different latitudes within 10-yr time windows (Fig. 3a), the contributions of solar activity (Fig. 3b), ENSO (Fig. 3c), and GHGs (Fig. 3e), and the values of the solar activity contributions relative to those of ENSO (Fig. 3d) and GHGs (Fig. 3f).

Overall, the 10-yr temperature trends fluctuate with the amplitude of about 0.5 K/decade at the tropical and the middle latitudes and about 1 K/decade at the polar latitudes. The solar activity contributions fluctuate (see the solid lines in Fig. 4 for a detailed illustration)with the amplitude of about

0.06 K/decade at the polar latitudes, 0.04 K/decade at the tropical latitudes, 0.01 K/decade at the northern middle latitudes, and 0.003 K/decade for the southern middle latitudes. So, the solar activity contributions are relatively small at all latitudes. The ENSO contributions vary (the dashed lines in Fig. 4) with the amplitude of about 0.15 K/decade at the polar latitudes, 0.06 K/decade at the tropical and the northern middle latitudes, and 0.01 K/decade at the southern middle latitudes. So, the contribution of ENSO is greater in amplitude than that of the solar activity, but still quite moderate. Figure 4 shows that both contributions are most close to each other at the tropical latitudes, while the ENSO contribution essentially dominates at the extratropical latitudes. However, the ratio of the solar activity contribution to that of ENSO can be quite different on different time intervals and sometimes much greater than unity, because the intervals of close-to-zero values are different for the solar activity and the ENSO contributions. For example, the solar activity contribution equals 0.02 K/decade on the interval [1997, 2006], where the ENSO contribution is 0.0006 K/decade.

Both the solar activity and the ENSO contributions are less than the GHGs contributions (Fig. 3e) even at the short time scale under consideration, except for the Antarctic region where the GHGs contribution is even less in amplitude than the two other contributions. Still, the solar activity contribution is not negligibly small in comparison with the significant GHGs contributions (Fig. 3f). We note that the sum of the contributions of the three factors included into the model (1) is usually not equal to the temperature trend itself. According to the model (1), the difference is due to the contribution of the noise ξ_n, examples of such noise realizations are shown in Fig. 2.

As for the longer time scales, our analysis within the time windows with $L_{end} = 2012$ and different lengths shows that both the ENSO and the solar activity contributions are much weaker than the GHGs contribution for time windows longer than 10 years. However, the role of the solar activity relative to the ENSO is dominating for the time windows longer than 80 years and at least comparable for shorter time scales. The corresponding results are presented in more detail in Sect. 4.3.

The results are similar for the AR models (1) with any other natural mode instead of the ENSO. Hence, the solar activity contribution may seem potentially significant at the first glance. Indeed, the solar activity variations were estimated as a sufficiently important factor in many previous studies where different data versions on different time intervals were analyzed with different methods. Below, we check this preliminary conclusion via assessing statistical significance of the coupling coefficient estimates and comparing of the AR models (1) and (2), i.e. with and without the solar activity variations.

4.2. AR Model Coefficients

Table 1 presents estimates of the two coefficients in the AR models (1) (upper number in each cell) and the AR models (2) (lower number in parentheses in each cell) which characterize sensitivity of the temperature anomalies T to the changes of the GHGs radiative forcing I_{GHG} and the natural variability indices I_M for the entire period since 1880 till 2012. One can see that almost all coefficients are the same for the models (1) and (2). Only some of them slightly decrease in absolute value (by one decimal digit in the lowest order) when the solar activity is taken into account, while the others remain unchanged under the accuracy used in Table 1. It means that the account of the solar activity variations practically does not change the estimates of the temperature sensitivities to the GHGs and the natural variability modes. The latter were discussed in (Mokhov & Smirnov, 2022) and are summarized below along with the new results for the temperature sensitivities to the insolation variations. Note that other choices of the estimation period are possible, e.g. the periods before 1950 and after 1950 would give two different sets of AR model coefficients. However, here we perform the analysis in a minimalistic spirit focusing on the question of contributions to the trend for the simplest possible model (1) with constant parameters. Using different estimation periods would correspond to the model with time-varying coefficient which is a more sophisticated case. Moreover, it can lead also to worse statistical reliability of the results due to the reduction of the data amount. It would be resonable to

Table 2

Estimates of the solar activity coupling coefficient a_4 with 95% confidence intervals for the AR models (1)

Lat	Coefficients of AR models: for the solar activity (a_4) andfor a natural variability mode (a_3)									
	AMO		ENSO		IPO		PDO		AAO	
	$a_4 \pm \Delta a_4$	$a_3 \pm \Delta a_3$	$a_4 \pm \Delta a_4$	$a_3 \pm \Delta a_3$	$a_4 \pm \Delta a_4$	$a_3 \pm \Delta a_3$	$a_4 \pm \Delta a_4$	$a_3 \pm \Delta a_3$	$a_4 \pm \Delta a_4$	$a_3 \pm \Delta a_3$
1	0.20 ± 1.40	**0.70** ± 0.50	0.26 ± 1.40	*0.09* ± 0.12	0.36 ± 1.40	*0.08* ± 0.11	0.30 ± 1.40	0.03 ± 0.07	0.28 ± 1.40	–0.015 ± 0.09
2	0.04 ± 0.63	**0.44** ± 0.25	0.05 ± 0.65	0.03 ± 0.06	0.07 ± 0.66	0.02 ± 0.05	0.06 ± 0.66	0.01 ± 0.03	0.06 ± 0.66	0.01 ± 0.04
3	0.13 ± 0.51	**0.23** ± 0.20	0.14 ± 0.51	*0.04* ± 0.05	0.16 ± 0.52	0.02 ± 0.05	0.14 ± 0.52	–0.00 ± 0.03	0.13 ± 0.51	***–0.03*** ± 0.03
4	0.20 ± 0.51	0.07 ± 0.18	0.20 ± 0.51	*0.04* ± 0.05	0.23 ± 0.51	0.02 ± 0.04	0.21 ± 0.51	–0.00 ± 0.03	0.21 ± 0.51	–0.02 ± 0.03
5	0.01 ± 0.30	0.00 ± 0.10	0.01 ± 0.30	–0.00 ± 0.03	0.01 ± 0.30	0.00 ± 0.02	0.01 ± 0.30	0.01 ± 0.02	0.02 ± 0.30	0.01 ± 0.02
6	0.30 ± 1.50	–0.05 ± 0.50	0.33 ± 1.50	***–0.11*** ± 0.12	0.24 ± 1.50	–0.05 ± 0.12	0.29 ± 1.50	–0.01 ± 0.07	0.28 ± 1.50	–0.05 ± 0.10

Notations are the same as in Table 1. The coefficient a_4 has the units of $K/(Wm^{-2})$, its values are shown together with a_3 for comparison

Table 3

Granger causality estimates as the mean-squared prediction improvements (PIs, measured in %) for the AR models with P = 1

Lat	$PI_{GHG \to T}$	$PI_{Sun \to T \mid GHG}$	$PI_{AMO \to T \mid GHG,Sun}$	$PI_{ENSO \to T \mid GHG,Sun}$	$PI_{IPO \to T \mid GHG,Sun}$	$PI_{PDO \to T \mid GHG,Sun}$	$PI_{AAO \to T \mid GHG,Sun}$
1	**25**	0.1	**5.7**	*1.8*	*1.4*	0.5	0.08
2	**21**	0.02	**8.6**	0.7	0.3	0.09	0.2
3	**21**	0.2	**4.2**	*1.6*	0.5	0.006	***2.8***
4	**24**	0.5	0.4	*1.6*	0.009	0.006	1.0
5	**11**	0.005	0.003	0.06	0.001	0.5	0.5
6	**3.9**	0.1	0.03	***2.2***	0.7	0.06	0.8

The GHGs PIs are given for the bivariate models (3), the solar activity PIs–for the trivariate models (3), the natural modes PIs–for the four-variate models (3). Meaning of the fonts is the same as in Table 1 indicating significance of the nonzero PI inference

Table 4

Estimates of the relative GHGs contributions C_{GHG}/α_T for the AR models (1) with solar activity (upper row in each cell) and the AR models (2) without solar activity (lower row in each cell).

Lat	20 years	30 years	50 years	130 years
1	0.33, 0.33, 0.33, 0.33, 0.34	0.41, 0.41, 0.41, 0.41, 0.42	0.62, 0.62, 0.63, 0.63, 0.64	0.96, 0.96, 0.97, 0.96, 0.99
	(0.33, 0.33, 0.34, 0.34, 0.35)	(0.41, 0.42, 0.43, 0.42, 0.43)	(0.64, 0.64, 0.66, 0.64, 0.66)	(0.98, 0.98, 1.01, 0.99, 1.02)
2	0.41, 0.41, 0.41, 0.41, 0.39	0.44, 0.45, 0.45, 0.45, 0.43	0.68, 0.69, 0.69, 0.69, 0.65	0.99, 0.99, 1.00, 1.00, 0.95
	(0.41,0.41, 0.42, 0.42, 0.40)	(0.44, 0.45, 0.46, 0.45, 0.43)	(0.68, 0.69, 0.70, 0.70, 0.66)	(0.99, 1.00, 1.01, 1.01, 0.96)
3	0.59, 0.59, 0.60, 0.59, 0.69	0.69, 0.69, 0.70, 0.69, 0.81 (0.71,	0.84, 0.83, 0.85, 0.84, 0.98	0.96, 0.95, 0.96, 0.96, 1.11
	(0.61, 0.61, 0.62, 0.61, 0.71)	0.71, 0.72, 0.72, 0.83)	(0.86, 0.86, 0.88, 0.87, 1.00)	(0.98, 0.98, 1.00, 0.99, 1.14)
4	0.96, 0.96, 0.97, 0.96, 1.03	1.18, 1.17, 1.18, 1.18, 1.26	0.92, 0.91, 0.92, 0.91, 0.98	0.97, 0.97, 0.97, 0.97, 1.04
	(1.00, 0.99, 1.01,1.00, 1.07)	(1.22, 1.21, 1.23, 1.23, 1.32)	(0.95, 0.95, 0.96, 0.95, 1.02)	(1.01, 1.00, 1.02, 1.01, 1.08)
5	1.37, 1.37, 1.38, 1.39, 1.25	1.85, 1.85, 1.85, 1.87, 1.68	1.15, 1.15, 1.15, 1.15, 1.04	1.01, 1.01, 1.01, 1.02, 0.92
	(1.38, 1.38, 1.39, 1.40, 1.26)	(1.86, 1.86, 1.86, 1.88, 1.70)	(1.15, 1.16, 1.16, 1.16, 1.06)	(1.02, 1.02, 1.02, 1.02, 0.93)
6	–0.46,–0.47, –0.44, –0.46, –0.66	–0.61, –0.62, –0.58, –0.60, –0.87	1.67, 1.71, 1.60, 1.66, 2.38	1.23, 1.26, 1.18, 1.22, 1.76
	(–0.52, –0.53, –0.49, –0.52, –0.71)	(–0.68, –0.70, –0.65, –0.68, –0.94)	(1.87, 1.93, 1.77, 1.86, 2.58)	(1.38, 1.42, 1.30, 1.37, 1.90)

Five numbers in each row of each cell correspond to the models accounting for AMO, ENSO, IPO, PDO, and AAO, respectively. The four columns show the results for the four different window lengths with the same window end point $L_{end} = 2012$

check such more complex models at the next steps of the investigation. The present study can then be used as a reference point to compare the results of the more complex models.

In going from an AR model (2) without the solar radiative forcing to an AR model (1), the coefficient a_2 representing the impact of GHGs changes by 10 to 12% for the Antarctic latitudes and by 3% for the Arctic latitudes and remains the same for all other latitudes. Just to repeat the previous result (Mokhov & Smirnov, 2022), it is always significant at least at the level of $p < 0.05$, i.e. its estimate exceeds twice the standard error estimate, and the largest value $a_2 = 0.35\ K/(Wm^{-2})$ is achieved for the Arctic latitudes.

According to the estimates of a_3 for the AMO, it does not change at all between the models (1) and (2), i.e. insensitive to the account of the solar radiative forcing in the model. We just repeat that the impact of AMO is essential only in the NH with the largest (and significant at the level of $p < 0.05$) value of $a_3 = 0.7$ for the Arctic latitudes.

Similalry, the estimates of a_3 do not change between the models (1) and (2) for ENSO, PDO, and AAO. We again repeat that the impact of ENSO is strongest at the polar latitudes with significance levels of $p = 0.1$ for the Antarctic and $p = 0.13$ for the Arctic. For the PDO, the estimates of a_3 are not significant even at $p = 0.2$. For the AAO, that estimate is significant at the tropical latitudes of NH ($p = 0.06$) and insignificant at the others.

The estimated coefficient a_3 for the IPO changes between the models (1) and (2) by 12 to 16% for the polar latitudes and remains unchanged for the other latitudes. We here repeat that its estimates are overall insignificant. It is interesting that multiple above mentioned insignificant estimates are not affected by the account of the solar radiative forcing in the models.

Table 2 presents the estimates of the solar activity coupling coefficient a_4 in the AR models (1) which characterizes the sensitivity of the temperatures to the solar activity variations. The values of a_3 are shown just for convenience of comparison of the confidence intervals, i.e. of statistical significance of the nonzero coefficients for the solar activity variations and the natural variability modes. One can see that the values of a_4 are always not significant even at the level of

Table 5

Estimates of the relative contributions of AMO, ENSO, IPO, PDO, and AAO to the temperature trends for the AR models (1) with solar activity (upper number in each cell) and the AR models (2) without solar activity (lower number in each cell)

Lat	C_{AMO}/α_T				C_{ENSO}/α_T				C_{IPO}/α_T				C_{PDO}/α_T				C_{AAO}/α_T			
	20	30	50	130	20	30	50	130	20	30	50	130	20	30	50	130	20	30	50	130
1	**0.33**	**0.28**	**0.11**	0.03	**–0.10**	–0.03	–0.00	0.01	**–0.11**	–0.07	0.00	–0.03	–0.06	–0.05	–0.00	–0.00	–0.02	–0.02	–0.03	–0.03
	(0.33)	**(0.28)**	**(0.11)**	(0.03)	**(–0.10)**	(–0.03)	(–0.00)	(0.01)	**(–0.11)**	(–0.06)	(0.00)	(–0.02)	(–0.06)	(–0.05)	(–0.00)	(–0.00)	(–0.02)	(–0.02)	(–0.03)	(–0.03)
2	**0.42**	**0.31**	**0.12**	0.03	–0.06	–0.02	0.00	0.01	–0.05	–0.03	0.00	–0.01	–0.03	–0.02	–0.00	–0.00	0.04	0.03	0.04	0.04
	(0.42)	**(0.31)**	**(0.12)**	(0.03)	(–0.06)	(–0.02)	(0.00)	(0.01)	(–0.06)	(–0.03)	(0.00)	(–0.01)	(–0.03)	(–0.02)	(–0.00)	(–0.00)	(0.04)	(0.03)	(0.04)	(0.04)
3	**0.44**	**0.35**	**0.10**	0.02	**–0.13**	–0.04	0.00	0.01	–0.10	–0.06	0.00	–0.01	–0.01	–0.01	–0.00	–0.00	**–0.19**	**–0.18**	**–0.18**	**–0.14**
	(0.45)	**(0.36)**	**(0.10)**	(0.02)	**(–0.13)**	(–0.04)	(0.00)	(0.01)	(–0.09)	(–0.05)	(0.00)	(–0.01)	(–0.01)	(–0.01)	(–0.00)	(–0.00)	**(–0.19)**	**(–0.18)**	**(–0.18)**	**(–0.14)**
4	0.20	0.16	0.03	0.01	**–0.18**	–0.06	0.00	0.01	*–0.14*	–0.08	0.00	–0.01	0.04	0.03	0.00	0.00	*–0.14*	*–0.14*	–0.09	–0.07
	(0.20)	(0.17)	(0.03)	(0.01)	**(–0.18)**	(–0.06)	(0.00)	(0.01)	*(–0.12)*	(–0.08)	(0.00)	(–0.01)	(0.04)	(0.04)	(0.00)	(0.00)	*(–0.15)*	*(–0.14)*	(–0.09)	(–0.07)
5	0.03	0.03	0.00	0.00	0.04	0.01	–0.00	–0.00	–0.01	–0.01	0.00	–0.00	*–0.18*	*–0.16*	0.01	–0.00	*0.20*	*0.25*	*0.12*	0.08
	(0.03)	(0.03)	(0.00)	(0.00)	(0.04)	(0.01)	(–0.00)	(–0.00)	(–0.01)	(–0.01)	(0.00)	(–0.00)	*(–0.19)*	*(–0.16)*	(0.01)	(–0.00)	*(0.20)*	*(0.25)*	*(0.12)*	(0.08)
6	*0.16*	*0.14*	–0.10	–0.01	**–0.68**	**–0.25**	0.02	–0.05	*–0.48*	*–0.30*	–0.01	*0.10*	*–0.12*	*–0.12*	0.01	0.01	*0.43*	*0.40*	*–0.97*	*–0.50*
	(0.14)	*(0.13)*	(–0.09)	(–0.01)	**(–0.67)**	**(–0.25)**	(0.02)	(–0.05)	*(–0.49)*	*(–0.31)*	(–0.01)	*(0.10)*	*(–0.13)*	*(–0.12)*	(0.01)	(0.01)	*(0.44)*	*(0.40)*	*(–0.98)*	*(–0.50)*

Each estimate is reported for the four window lengths (20, 30, 50, and 130 years) with the same window end point $L_{end} = 2012$. Fonts are the same as in Table 1

$p < 0.3$, i.e. they are always less than the standard error estimate (less than "1σ") and often much less. The largest ratio of the a_4 estimate to its standard error is obtained for the tropical latitudes of the SH (a_4 is about 0.8), while the next large values are obtained for the NH tropical latitudes, Antarctic and Arctic latitudes (about 0.4–0.5). For the NH middle latitudes, we get a_4 about 0.2 and even less a_4 of about 0.06 for the SH middle latitudes. Hence, all estimates of the solar activity contributions to the temperature trends presented in Sect. 4.1 (above) and 4.3 (below) are also non-significant and can be provided with the corresponding relative values of the confidence intervals. If one still tries to extract "most considerable" numerical estimates, the solar activity contributions to the tropical temperature trends should be considered first, while the estimates for the polar latitudes are even less reliable and those for the middle latitudes should be neglected.

Table 3 presents the estimates of the Granger causality in terms of the mean-squared PI, just to give an alternative numerical expression of the different influences on the temperatures. These estimates confirm the strongest role of the GHGs at all latitudes with its relatively smaller PIs at the southern middle and polar latitudes, an insigninficant role of the solar radiative forcing at all latitudes, a strong role of AMO in the NH, a quite notable role of ENSO in the polar regions, a quite notable role of AAO in the northern tropics and its somewhat weaker role in the southern tropics, a weak role of IPO in Arctic, an absent role of PDO at all latitudes, and an absent influence of all factors (except for the GHGs) in the southern middle latitudes.

4.3. *Contributions of Various Factors to the Temperature Trends*

As a consequence of the above independence of the coefficients a_2 and a_3 on the inclusion or non-inclusion of the solar activity into the AR models (Table 1), the estimates of the contributions of the GHGs and natural variability modes to the temperature trends do not depend on the account of the solar activity as well, see Tables 4 and 5 where those two contributions are shown for the time windows of the lengths ranging from 10 to 130 years. The lower

Table 6

Estimates of the relative contributions of the solar activity C_{Sun}/α_T and its ratio to the contributions of the natural variability modes C_{Sun}/C_{AMO},C_{Sun}/C_{ENSO},C_{Sun}/C_{IPO},C_{Sun}/C_{PDO}, and C_{Sun}/C_{AAO}(in parentheses) according to the AR models (1) for the four window lengths (20, 30, 50, and 130 years) with the same window end point $L_{end} = 2012$

Lat	20 years	30 years	50 years	130 years
1	–0.01, –0.01,– 0.02, –0.02, –0.02	–0.01, –0.01, –0.01, –0.01, –0.01	0.00, 0.00, 0.01, 0.01, 0.01	0.02, 0.03, 0.04, 0.03, 0.03 (0.67, 3.50, –1.70, –10.0, –1.20)
	(–0.03, 0.15, 0.18, 0.28, 0.73)	(–0.02, 0.27, 0.19, 0.20, 0.51)	(0.03, –7.30, 2.80, –1.90, –0.19)	
2	–0.00,– 0.01, –0.01, –0.01, –0.01	–0.00, –0.00, –0.01, –0.00, –0.01	0.00, 0.00, 0.00, 0.00, 0.00	0.01, 0.01, 0.02, 0.01, 0.01 (–0.23, 2.10, –1.60, –12.0, 0.33)
	(–0.01, 0.12, 0.19, 0.31, –0.22)	(–0.01, 0.21, 0.20,0.21, –0.14)	(–0.01, 2.40, 1.10, –2.90, 0.05)	
3	–0.03, –0.03, –0.04, –0.03, –0.03	–0.02, –0.02, –0.02, –0.02, –0.02	0.01, 0.01, 0.01, 0.01, 0.01	0.03, 0.04, 0.04, 0.04, 0.04 (1.40, 4.50, –3.20, –143.0, –0.26)
	(–0.06, 0.23, 0.37, 3.40, 0.17)	(–0.05, 0.41, 0.38, 2.30, 0.11)	(0.06, 12.0, 2.50, –33.0, –0.04)	
4	–0.07, –0.06, –0.07, –0.07, –0.07	–0.04, –0.04, –0.04, –0.04, –0.04	0.01, 0.01, 0.01, 0.01, 0.01	0.05, 0.04, 0.05, 0.05, 0.05 (8.10, 6.50, –4.50, 72.0, –0.73)
	(–0.34, 0.32,0.53, –1.80, 0.48)	(–0.25, 0.57, 0.55, –1.20, 0.31)	(0.30, 36.0, 4.10, 16.0, –0.10)	
5	–0.01, –0.01, –0.01, –0.01, –0.01	–0.01, –0.01, –0.01, –0.01, –0.01	0.00, 0.00, 0.00, 0.00, 0.00	0.01, 0.01, 0.01, 0.01, 0.01
	(–0.29, –0.28, 0.97, 0.04,–0.07)	(–0.28, –0.58, 1.11, 0.03, –0.04)	(1.05, –0.76, 2.20, 0.15, 0.02)	(25.0, –4.2, –12.0, –59.0, 0.17)
6	0.09, 0.10, 0.07, 0.09, 0.08	0.06, 0.07, 0.05, 0.06, 0.06	0.06, 0.06, 0.05, 0.06, 0.05	0.18, 0.20, 0.15, 0.18, 0.17
	(0.58, –0.15, –0.15,–0.70, 0.19)	(0.43, –0.27, –0.17, –0.51, 0.14)	(–0.57,3.50, –5.20, 4.90, –0.06)	(–14.0, –4.0, 1.60, 26.0, –0.35)

numbers in each cell (in parentheses) correspond to the AR models (2), and they are quite close to the upper numbers corresponding to the AR models (1). The main points can be summarized as follows.

The estimates of the GHGs contribution C_{GHG}/α_T are most strongly influenced by the account of the solar activity for the Antarctic latitudes (Table 4). Namely, inclusion of the solar activity into the AR model leads to the relative decrease of C_{GHG}/α_T by about 10%. For the tropical latitudes of the SH, this decrease is about 4–6%. It is about 2–4% for the tropical and polar latitudes of the NH and about 1% for the middle latitudes of both hemispheres.

Table 5 presents the relative contributions of the five climatic modes for the AR models (1) and (2). For that finite accuracy, the ratios C_{AMO}/α_T, C_{ENSO}/α_T, C_{IPO}/α_T, C_{PDO}/α_T, and C_{AAO}/α_T either remain unchanged or decrease by one decimal digit after the inclusion of the solar activity into the AR model. Only two numbers change in two decimal digits. All these estimates are affected by 10% or less under the account of the solar activity.

Table 6 presents the relative contributions of the solar activity to the temperature trends. The numerical values (upper row of numbers in each cell) are mainly quite small. They are less than 0.05 except for the Antarctic latitudes,where they exceed 0.1 and reach 0.2 for the long time windows. These values for the tropical latitudes (about 0.05) are greater than those for the Arctic and middle latitudes (about 0.01 to 0.02). It is worth to note the non-monotone dependence on the window length: the weakest contributions are observed for the time windows of the length of 50 years, while the larger values for the longer windows are explained by the long-term trend in the time series of solar activity variations which leads to the dominance of the solar activity contributions over natural variability modes at large enough time scale. One can also notice that the solar activity contributions to the temperature trends at different latitudes (except for the Antarctic ones) are negative on shorter time intervals of the two or three decades, while they are positive on the intervals of half a century and longer. Still, all these observations correspond to quite weakly significant estimates of the solar activity influence on the temperature trends. To be cautious, one must conclude that a reliable

detection of the solar activity contributions to temperature trends from the data at hand is not possible. So, the previous estimates of the contributions of the GHGs and natural variability modes (Mokhov & Smirnov, 2022) remain almost unchanged under the account of the solar activity and so their reliability is confirmed.

5. Conclusions

Quantitative estimates of the contribution of insolation variations to surface air temperature trends in tropical, middle and polar latitudes over time intervals from a decade to a century have been obtained with the use of multivariate AR models and the respective short-term (Granger) and long-term causality characteristics based on observational data since the nineteenth century. This is done with minimal assumptions about the data used and the empirical models fitted to the data. According to the presented results, the contributions of the insolation variations to the trends of the surface air temperatures are statistically insignificant at time intervals longer than two decades. Sensitivity of the temperature variations to the insolation interdecadal variations is less statistically significant than this sensitivity to the other factors including anthropogenic influences and natural variability modes.

According to the numerical values of the obtained estimates, the contributions of the insolation variations to the temperature trends at different latitudes for some time intervals can considerably exceed the respective estimates of the contributions of the natural variability modes. It is found that the contributions of the insolation variations to the temperature trends can reach 7% at the tropical latitudes and 10% at the Antarctic latitudes with the smallest values at the middle latitudes. It is noted that for the most recent, relatively short time intervals (within three decades), these contributions at different latitudes (except for the Antarctic ones) is negative, while for half a century and longer time intervals they are positive. The account of the insolation variations in the AR models weakly (by several per cent or less) changes the estimates of the contributions of the GHGs and natural variability modes to the temperature trends at different latitudes.

Author contribution Both authors contributed to the study design and data analysis. Both authors wrote the main manuscript text, reviewed the manuscript and approved the final manuscript.

Funding

This study was supported by the Russian Science Foundation project No. 19–17-00240. The results obtained within the framework of the RSF-NSFC project 23-47-00104 were also used

Data availability statement

The data used for the analysis are available at (GISS, 2018; Huang et al., 2015; NCEI, 2022; PSL, 2022).

Declarations

Conflict of interest The authors declare they have no financial interests.

References

Allen, M. R., Gillett, N. P., Kettleborough, J. A., Hegerl, G., Schnur, R., Stott, P. A., Boer, G., Covey, C., Delworth, T. L., Jones, G. S., & Mitchell, J. F. (2006). Quantifying anthropogenic influence on recent near-surface temperature change. *Surveys in Geophysics, 27*, 491–544.

Allen, M. R., & Stott, P. A. (2003). Estimating signal amplitudes in optimal fingerprinting, part I: Theory. *Climate Dynamics, 21*, 477–491.

Allen, M. R., & Tett, S. F. B. (1999). Checking for model consistency in optimal fingerprinting. *Climate Dynamics, 15*, 419–434.

Anet, J. G., Rozanov, E. V., Muthers, S., Peter, T., Brönnimann, S., Arfeuille, F., Beer, J., Shapiro, A. I., Raible, C. C., Steinhilber, F., & Schmutz, W. K. (2013). Impact of a potential 21st century "grand solar minimum" on surface temperatures and stratospheric ozone. *Geophysical Research Letters, 40*, 4420–4425.

Arsenovic, P., Rozanov, E., Anet, J., Stenke, A., Schmutz, W., & Peter, T. (2018). Implications of potential future grand solar minimum for ozone layer and climate. *Atmospheric and Chemical Physics, 18*, 3469–3483.

Attanasio, A., & Triacca, U. (2011). Detecting human influence on climate using neural networks based Granger causality. *Theoretical and Applied Climatology, 103*(1–2), 103–107.

Bindoff, N. L., Stott, P. A., AchutaRao, K. M., Allen, M. R., Gillett, N., Gutzler, D., Hansingo, K., Hegerl, G., Hu, Y., Jain, S., II., Overland, M. J., Perlwitz, J., Sebbari, R., & Zhang, X. (2013). *In: Climate Change 2013: The physical science basis. Contribution of working group I to the fifth assessment report of the intergovernmental panel on climate change* (pp. 867–952). Cambridge University Press.

Enfield, D. B., Mestas-Nunez, A. M., & Trimble, P. J. (2001). The Atlantic Multidecadal Oscillation and its relationship to rainfall and river flows in the continental U.S. *Geophysical Research Letters, 28*, 2077–2080.

Feulner, G., & Rahmstorf, S. (2010). On the effect of a new grand minimum of solar activity on the future climate on Earth. *Geophysical Research Letters, 37*(5), L05707.

Foster, G., & Rahmstorf, S. (2011). Global temperature evolution 1979–2010. *Environmental Research Letters, 6*, 044022.

GISS, (2018). Forcings in climate models. national aeronautics and space administration, goddard institute for space studies. (https://data.giss.nasa.gov/modelforce/Miller_et_2014/Fi_Miller_et_al14_upd.txt).

Gong, D., & Wang, S. (1999). Definition of Antarctic oscillation index. *Geophysical Research Letters, 26*(4), 459–462.

Granger, C. W. J. (1963). Economic processes involving feedback. *Information and Control, 6*, 28.

Granger, C. W. J. (1969). Investigating causal relations by econometric models and cross-spectral methods. *Econometrica, 37*(3), 424–438.

Gruza, G. V., & Rankova, E. Y. A. (2012). *Observed and expected climate changes over Russia: Surface and temperature*. RIHMI-WDC. (in Russian).

Hasselmann, K. (1993). Optimal fingerprints for the detection of time-dependent climate change. *Journal of Climate, 6*, 1957–1971.

Hasselmann, K. (1997). Multi-pattern fingerprint method for detection and attribution of climate change. *Climate Dynamics, 13*, 601–611.

Hegerl, G. C., von Storch, H., Hasselmann, K., Santer, B. D., Cubasch, U., & Jones, P. D. (1996). Detecting greenhouse-gas-induced climate change with an optimal fingerprint method. *Journal of Climate, 9*, 2281–2306.

Hegerl, G. C., & Zwiers, F. (2011). Use of models in detection and attribution of climate change. *Wires Climate Change, 2*, 570–591.

Henley, B. J., Gergis, J., Karoly, D. J., Power, S. B., Kennedy, J., & Folland, C. K. (2015). A tripole index for the interdecadal pacific oscillation. *Climate Dynamics, 45*(11–12), 3077–3090.

Huang, B., Banzon, V. F., Freeman, E., Lawrimore, J., Liu, W., Peterson, T. C., Smith, T. M., Thorne, P. W., Woodruff, S. D., & Zhang, H.-M. (2014). Extended reconstructed sea surface temperature version 4 (ERSST.v4): Part I. Upgrades and intercomparisons. *Journal of Climate, 28*, 911–930.

Huang, B., Banzon, V.F., Freeman, E., Lawrimore, J., Liu, W., Peterson, T.C., Smith, T.M., Thorne, P.W., Woodruff, S.D., and Zhang, H.-M. (2015). Extended reconstructed sea surface temperature (ERSST), Version 4. NOAA National Centers for Environmental Information. https://doi.org/10.7289/V5KD1VVF (ftp://ftp.ncdc.noaa.gov/pub/data/noaaglobaltemp/operational/timeseries/).

Huntingford, C., Stott, P. A., Allen, M. R., & Lambert, F. H. (2006). Incorporating model uncertainty into attribution of observed temperature change. *Geophysical Research Letters, 33*, L05710.

Imbers, J., Lopez, A., Huntingford, C., & Allen, M. R. (2013). Testing the robustness of the anthropogenic climate change detection statements using different empirical models. *Journal of Geophysical Research Atmospheres, 118*, 3192–3199.

Imbers, J., Lopez, A., Huntingford, C., & Allen, M. R. (2014). Sensitivity of climate change detection and attribution to the characterization of internal climate variability. *Journal of Climate, 27*, 3477–3491.

Jia, L., & DelSole, T. (2012). Optimal determination of time-varying climate change signals. *Journal of Climate, 25*, 7122–7137.

Jones, G. S., Lockwood, M., & Stott, P. A. (2012). What influence will future solar activity changes over the 21st century have on projected global near-surface temperature changes? *Journal of Geophysical Research, 117*, D05103. https://doi.org/10.1029/2011JD017013

Kajtar, J. B., Collins, M., Frankcombe, L. M., England, M. H., Osborn, T. J., & Juniper, M. (2019). Global mean surface temperature response to large-scale patterns of variability in observations and CMIP5. *Geophysical Research Letters, 46*, 2232–2241.

Kaufmann, R., Kauppi, H., Mann, M., & Stock, J. (2011). Reconciling anthropogenic climate change with observed temperature 1998–2008. *Proceedings of the National Academy of Sciences, 108*, 11790–11793.

Kaufmann, R., Kauppi, H., & Stock, J. (2006). Emissions, concentrations, & temperature: A time series analysis. *Climatic Change, 77*, 249–278.

Kaufmann, R. K., & Stern, D. I. (1997). Evidence for human influence on climate from hemispheric temperature relations. *Nature, 388*, 39–44.

Kodra, E., Chatterjee, S., & Ganguly, A. R. (2011). Exploring Granger causality between global average observed time series of carbon dioxide and temperature. *Theoretical and Applied Climatology, 104*(3–4), 325–335.

Kopp, G., & Lean, J. (2011). A new, lower value of total solar irradiance: Evidence and climate significance. *Geophysical Research Letters, 38*, L01706.

Lean, J. L., & Rind, D. H. (2008). How natural and anthropogenic influences alter global and regional surface temperatures: 1889 to 2006. *Geophysical Research Letters, 35*, L18701.

Lean, J. L., & Rind, D. H. (2009). How will Earth's surface temperature change in future decades? *Geophysical Research Letters, 36*, L15708.

Liu, W., Huang, B., Thorne, P. W., Banzon, V. F., Zhang, H. M., Freeman, E., Lawrimore, J., Peterson, T. C., Smith, T. M., & Woodruff, S. D. (2014). Extended reconstructed Sea surface temperature version 4 (ERSST.v4): Part II. Parametric and structural uncertainty estimations. *Journal of Climate, 28*, 931–951.

Lockwood, M. (2008). Recent changes in solar outputs and the global mean surface temperature. III. Analysis of contributions to global mean air surface temperature rise. *Proceedings of the Royal Society A Mathematical Physical and Engineering Sciences, 464*(2094), 1387–1404.

Loehle, C., & Scafetta, N. (2011). Climate change attribution using empirical decomposition of climatic data. *Open Atmospheric Science Journal, 5*, 74–86.

Masson-Delmotte, V., Zhai, P., Pirani, A., Connors, S. L., Péan, C., Berger, S., Caud, N., Chen, Y., Goldfarb, L., Gomis, M. I., Huang, M., Leitzell, K., Lonnoy, E., Matthews, J. B. R., Maycock, T. K., Waterfield, T., Yelekçi, O., Yu, R., & Zhou B. (eds.) (2021). *Climate Change 2021: the physical science basis. Contribution of working group I to the sixth assessment report of the intergovernmental panel on climate change.* Cambridge University Press.

Maycock, A. C., Ineson, S., Gray, L. J., Scaife, A. A., Anstey, J. A., Lockwood, M., Butchart, N., Hardiman, S. C., Mitchell, D. M., & Osprey, S. M. (2015). Possible impacts of a future grand solar minimum on climate: Stratospheric and global circulation changes. *Journal of Geophysical Research Atmospheres*. https://doi.org/10.1002/2014JD022022

McBride, L. A., Hope, A. P., Canty, T. P., Bennett, B. F., Tribett, W. R., & Salawitch, R. J. (2021). Comparison of CMIP6 historical climate simulations and future projected warming to an empirical model of global climate. *Earth System Dynamics, 12*, 545–579.

Meehl, G. A., Arblaster, J. M., & Marsh, D. R. (2013). Could a future "grand Solar Minimum" like Maunder Minimum stop global warming? *Geophysical Research Letters, 40*(1789), 1793.

Miller, R. L., Schmidt, G. A., Nazarenko, L. S., Tausnev, N., Bauer, S. E., DelGenio, A. D., Kelley, M., Lo, K. K., Ruedy, R., Shindell, D. T., & Aleinov, I. (2014). CMIP5 historical simulations (1850–2012) with GISS ModelE2. *Journal of Advances in Modeling Earth Systems, 6*(2), 441–477.

Mokhov, I. I., Bezverkhnii, V. A., Eliseev, A. V., & Karpenko, A. A. (2006). Model estimations of global climate changes in the 21st century with account for different variation scenarios of solar activity. *Doklady Earth Sciences, 411*(8), 1327–1330.

Mokhov, I. I., Bezverkhnii, V. A., Eliseev, A. V., & Karpenko, A. A. (2008). Model estimations of possible climatic changes in 21st century at different scenarios of solar and volcanic activities and anthropogenic impact. *Cosmic Research, 46*(4), 354–357.

Mokhov, I. I., & Smirnov, D. A. (2008). Diagnostics of a cause–effect relation between solar activity and the Earth's global surface temperature. *Izvestiya, Atmospheric and Oceanic Physics, 44*(3), 263–272.

Mokhov, I. I., & Smirnov, D. A. (2009). Empirical estimates of the influence of natural and anthropogenic factors on the global surface temperature. *Doklady Earth Sciences, 427*(1), 798–803.

Mokhov, I. I., & Smirnov, D. A. (2016). Relation between the variations in the global surface temperature, El Nino/La Nina phenomena, and the Atlantic Multidecadal Oscillation. *Doklady Earth Sciences, 467*(2), 384–388.

Mokhov, I. I., & Smirnov, D. A. (2016). The Trivariate Seasonal Analysis of Couplings between El Nino, North Atlantic Oscillation, and Indian Monsoon. *Russian Meteorology and Hydrology, 41*(11–12), 798–807.

Mokhov, I. I., & Smirnov, D. A. (2017). Estimates of mutual influences between sea surface temperature variations in tropical Pacific, Atlantic, and Indian oceans from long-period data series. *Izvestiya, Atmospheric and Oceanic Physics, 53*(6), 613–623.

Mokhov, I. I., & Smirnov, D. A. (2018). Estimating the contributions of the Atlantic Multidecadal Oscillation and variations in the atmospheric concentration of greenhouse gases to surface air temperature trends from observations. *Doklady Earth Sciences, 480*(1), 602–606.

Mokhov, I. I., & Smirnov, D. A. (2018). Contribution of greenhouse gas radiative forcingand Atlantic Multidecadal Oscillation to surface air temperature trends. *Russian Meteorology and Hydrology, 43*(9), 557–564.

Mokhov, I. I., & Smirnov, D. A. (2022). Contributions to surface air temperature trends estimated from climate time series: Medium-term causalities. *Chaos, 32*, 063128. https://doi.org/10.1063/5.0088042

Mokhov, I. I., Smirnov, D. A., & Karpenko, A. A. (2012). Assessments of the relationship of changes of the global surface air temperature with different natural and anthropogenic factors based on observations. *Doklady Earth Sciences, 443*(1), 381–387.

Mokhov, I. I., Smirnov, D. A., Nakonechny, P. I., Kozlenko, S. S., Seleznev, E. P., & Kurths, J. (2011). Alternating mutual influence of El-Nino/Southern Oscillation and Indian monsoon. *Geophysical Research Letters*. https://doi.org/10.1029/2010GL045932

Mukhin, D., Gavrilov, A., Seleznev, A., & Buyanova, M. (2021). An atmospheric signal lowering the spring predictability barrier in statistical ENSO forecasts. *Geophysical Research Letters, 48*(6), e2020GL091287. https://doi.org/10.1029/2020GL091287

NCEI. (2022). National Oceanic and Atmospheric Administration, National Centers for Environmental Information. (https://www.ncei.noaa.gov/pub/data/cmb/ersst/v5/index/ersst.v5.pdo.dat).

PSL, (2022). National Oceanic and Atmospheric Administration, Physical Sciences Laboratory. (AMO:http://www.esrl.noaa.gov/psd/data/correlation//amon.us.long.data; ENSO:https://psl.noaa.gov/gcos_wgsp/Timeseries/Data/nino34.long.anom.data; IPO:https://psl.noaa.gov/data/timeseries/IPOTPI/tpi.timeseries.hadisst1.1.data; AAO:https://psl.noaa.gov/data/20thC_Rean/timeseries/monthly/SAM/sam.20crv2.long.data).

Rayner, N. A., Parker, D. E., Horton, E. B., Folland, C. K., Alexander, L. V., Rowell, D. P., Kent, E. C., & Kaplan, A. (2003). Global analyses of sea surface temperature, sea ice, and night marine air temperature since the late nineteenth century. *Journal of Geophysical Research, 108*(D14), 4407.

Ribes, A., Azais, J.-M., & Planton, S. (2009). Adaptation of the optimal fingerprint method for climate change detection using a well-conditioned covariance matrix estimate. *Climate Dynamics, 33*, 707–722.

Ribes, A., & Terray, L. (2013). Application of regularised optimal fingerprinting to attribution. Part II: Application to global near-surface temperature. *Climate Dynamics, 41*, 2837–2853.

Santer, B. D., Wigley, T. M., Doutriaux, C., Boyle, J. S., Hansen, J. E., Jones, P. D., Meehl, G. A., Roeckner, E., Sengupta, S., & Taylor, K. E. (2001). Accounting for the effects of volcanoes and ENSO in comparisons of modeled and observed temperature

trends. *Journal of Geophysical Research, 106*(D22), 28033–28059.

Schwarz, G. (1978). Estimating the dimension of a model. *Annals of Statistics, 6*(2), 461–464.

Seleznev, A., Mukhin, D., Gavrilov, A., Loskutov, E., & Feigin, A. (2019). Bayesian framework for simulation of dynamical systems from multidimensional data using recurrent neural network. *Chaos, 29*(12), 123115.

Smirnov, D. A. (2014). Quantifying causal couplings via dynamical effects: A unifying perspective. *Physical Review E, 90*(6), 062921.

Smirnov, D. A. (2022). Generative formalism of causality quantifiers for processes. *Physical Review E, 105*(3), 034209.

Smirnov, D. A., & Mokhov, I. I. (2009). From Granger causality to "long-term causality": Application to climatic data. *Physical Review E, 80*(1), 016208.

Smirnov, D. A., & Mokhov, I. I. (2015). Relating Granger causality to long-term causal effects. *Physical Review E, 92*(4), 042138.

Song, X., Lubin, D., & Zhang, G. J. (2010). Increased greenhouse gases enhance regional climate response to a Maunder Minimum. *Geophysical Research Letters*, *37*, L01703. https://doi.org/10.1029/2009GL041290

Stern, D. I., & Kaufmann, R. K. (2014). Anthropogenic and natural causes of climate change. *Climatic Change, 122*, 257–269.

Stips, A., Macias, D., Coughlan, C., Garcia-Gorriz, E., & San Liang, X. (2016). On the causal structure between CO_2 and global temperature. *Scientific Reports, 6*, 21691.

Stocker, T. F., Qin, D., Plattner, G.-K., Tignor, M., Allen, S. K., Boschung, J., Nauels, A., Xia, Y., Bex, V., & Midgley, P. M. (Eds.) (2013). *Climate Change 2013: The physical science basis. Contribution of working group I to the fifth assessment report of the intergovernmental panel on climate change*. Cambridge University Press.

Stolpe, M. B., Medhaug, I., & Knutti, R. (2017). Contribution of Atlantic and Pacific multidecadal variability to twentieth-century temperature changes. *Journal of Climate, 30*, 6279–6295.

Tol, R. S. J., & de Vos, A. F. (1993). Greenhouse statistics–time series analysis. *Theoretical and Applied Climatology, 48*, 63–74.

Triacca, U., Attanasio, A., & Pasini, A. (2013). Anthropogenic global warming hypothesis: Testing its robustness by Granger causality analysis. *Environmetrics, 24*, 260–268.

Tung, K. K., & Camp, C. D. (2008). Solar cycle warming at the Earth's surface in NCEP and ERA-40 data: A linear discriminant analysis. *Journal of Geophysical Research, 113*, D05114.

Verdes, P. F. (2007). Global warming is driven by anthropogenic emissions: A time series analysis approach. *Physical Review Letters, 99*, 048501.

Zhou, J., & Tung, K. K. (2013). Deducing multidecadal anthropogenic global warming trends using multiple regression analysis. *Journal of the Atmospheric Sciences, 70*, 3–8.

(Received March 4, 2023, revised May 27, 2023, accepted June 15, 2023)